Monte Carlo Simulations of Stable Point Defects in Hybrid Nematic Films

C. Chiccoli,[1] O. D. Lavrentovich,[2] P. Pasini,[1] and C. Zannoni[3]
[1]*Istituto Nazionale di Fisica Nucleare, Sezione di Bologna, Via Irnerio 46, 40126 Bologna, Italy*
[2]*Liquid Crystal Institute and Chemical Physics Interdisciplinary Program, Kent State University, Kent, Ohio 44242*
[3]*Dipartimento di Chimica Fisica ed Inorganica, Università di Bologna, Viale Risorgimento 4, 40136 Bologna, Italy*
(Received 14 July 1997)

Monte Carlo (MC) simulations based exclusively on nearest-neighbor intermolecular interactions reveal the existence of stable long-range deformations and topological defects in a thin nematic film confined between two surfaces with antagonistic (normal and tangential) molecular orientations. Thus the MC technique allows one to describe a delicate balance of bulk elasticity and surface energy usually treated only with macroscopic theories. [S0031-9007(97)04727-3]

PACS numbers: 61.30.Cz, 61.30.Gd, 64.70.Md

There are three well-known mechanisms that lead to the formation of topologically stable defects [1] in systems with spontaneously broken symmetry. The first one is fast quench through phase transitions [2,3]. The defects appear as a result of the combination of domains with a different (but uniform within each domain) phase of the order parameter. These defects annihilate in the phase ordering process. Second, defect networks can emerge as stable structures to minimize the bulk energy. Well-known examples are Abrikosov lattices in superconductors and the so-called twist grain boundary [4,5] and blue phases [6] of liquid crystals (LC). In both the above mechanisms the presence of bounding surfaces plays no significant role in the formation of the defects. Contrary to this, in the third mechanism stable defects appear as a topological response of the system to a closed bounding surface. For example, for spherically bounded liquid crystal droplets the Poincaré and Gauss theorems guarantee the existence of defects provided the anisotropic surface energy WR^2 overweights the bulk elastic energy KR (i.e., the system size R is larger than $R_C = K/W$), where K is an effective elastic constant and W is the anchoring coefficient [7]. A similar phenomenon occurs when one disperses sufficiently large particles in the liquid crystal bulk [8]. The above topological mechanisms do not work, however, when the boundary is not closed or when the so-called Euler characteristic of the boundary is zero (as in the case of a torus).

In this Letter we report the results of Monte Carlo (MC) simulations with purely microscopic molecular interactions that show the appearance of stable topological defects for a system in which none of the above three mechanisms appears to be called to action. Defects appear in nematic films with hybrid boundary conditions when the film thickness h is much smaller than its lateral size L. Although similar results are established experimentally and on the basis of continuum theory [9], neither microscopic theory derivations nor computer simulations of such stable defects exist for this LC system. MC simulation is a particularly attractive technique to study defects [10], since it provides a way of determining equilibrium molecular organizations starting in principle from an arbitrary one. More interestingly the technique can be used to examine the relative stability of a configuration used as a starting one, to see if and how it evolves into another one of lower free energy.

Here we deal with a model where the molecules, assumed to be three dimensional "headless spins," lie on the sites of a cubic lattice and interact through the second rank Lebwohl-Lasher (LL) potential [11,12]:

$$U_{ij} = -\epsilon_{ij} P_2(\cos\beta_{ij}), \tag{1}$$

where ϵ_{ij} equals $\epsilon > 0$ for nearest-neighbor particles i and j and is zero otherwise, P_2 is the second rank Legendre polynomial, β_{ij} is the angle between the axis, $\mathbf{u}_i$, $\mathbf{u}_j$ of the two spins i, j representing a cluster of molecules whose short-range order is maintained through the temperature range examined [13]. The LL potential reproduces well the orientational ordering of a nematic and its transition to the isotropic phase [11,12].

The crucial feature of the present MC simulations is the type of boundary conditions (BC) imposed onto the system through layers of spins with suitably fixed orientations. We mimic a hybrid aligned nematic (HAN) cell [9]. The spins of the bottom layer, $z = 0$, have random fixed orientations in the horizontal (x, y) plane, while those of the top layer, $z = h$, are fixed along the surface normal. The anchoring of the liquid crystal to the surface spins is given by Eq. (1). Open BC, i.e., empty space, are assumed on the four planes surrounding the cell. MC calculations normally employ periodic BC with identical replicas surrounding the sample [14]. This artificial periodicity causes no fundamental artifacts in the modeling of uniform states. However, when the ground state contains topological defects, they might be incompatible with periodic BC and hence our reason for not using them.

Independent simulations for various lattice sizes have been performed using a standard canonical (constant number of spins N, volume V, and temperature $T^* = kT/\epsilon$) Metropolis algorithm [14] to update the lattice, as previously described in detail [10,12]. In particular we have investigated films containing six, eight, or ten layers in

addition to the two, top and bottom, fixed surfaces. The dependence on the system size has been investigated keeping the thickness h fixed and varying the side L of the square film. In particular considering ten layers along z, i.e., the two antagonistic surfaces and eight layers between them, we have varied the square size from 10×10 up to 60×60 with a step of 10. For systems up to $L = 30$ a wide range of temperatures (about 20) for each system has been investigated. We have calculated several thermodynamic observables: energy, heat capacity, second and fourth rank order parameters, and the orientational correlation functions. These results are complementary and will be reported elsewhere. Moreover simulations at selected temperatures have been performed for fairly large systems ($50 \times 50 \times 12$, $100 \times 100 \times 12$, $100 \times 100 \times 10$, $100 \times 100 \times 8$, and $100 \times 100 \times 6$).

Similarly to real experiments, the simulated textures are visualized through crossed polarizers. This approach has been employed in calculations based on continuum theory [15–17] and MC simulations [13,18]. We compute the optical patterns corresponding to the simulated configurations by using a Müller matrix approach and the same refractive and material parameters reported in [13]. The light retarded by the liquid crystal molecules in the HAN cell is observed with crossed polarizers placed at $\pi/4$ and $(3/4)\pi$ with respect to x. A pixel by pixel intensity map $I(x, y)$ is obtained and the calculation is then repeated over a number (typically 500) of different configurations sampled around a certain evolution step to give the average intensity maps shown with a grey coding in the figures (between black: no light, and white: light through) [13].

In a first set of computer experiments we have started the simulations from a configuration perfectly aligned along the z axis. As an example we report in Fig. 1 cross-polarizer images of various evolution stages for a $100 \times 100 \times 12$ lattice at $T^* = 0.4$. The texture develops from black to a set of brushes. Each defect is marked by four brushes emerging from its core [1]. The texture evolves as the system anneals, but the defects do not disappear even in the longest runs performed (120 000 cycles, where a cycle is a full lattice update) even though they occasionally migrate outside the sample. As for the effect of film size we notice that the defects do not seem to appear until the lateral size L becomes much larger than h (e.g., $L \geq 50$ for $h = 10$); see Fig. 2. We now examine the molecular organizations corresponding to the optical patterns. Figures 3 and 4 show molecular organizations for the textures of Fig. 2 for the films with small and large L/h, $10 \times 10 \times 10$ and $50 \times 50 \times 10$, respectively. In the film with small L/h, Fig. 3, the director is strongly deformed in the vertical plane, obviously following the antagonistic boundary conditions at $z = 0$ and $z = h$. The horizontal director field is uniform, although not perfectly: small variations of the director are visible in both Figs. 3 and 2 (top left). The situation dramatically changes for large L/h: in Figs. 4 and 2 (bottom left) one observes strong and stable horizontal deformations associated with topological defects. The defects are of strength $m = \pm 1$, i.e., the director field undergoes a $\pm 2\pi$ rotation as one goes once around the defect core. The absolute value $|m| = 1$ is the lowest possible topological charge of a defect in a HAN film. The core of the defect is

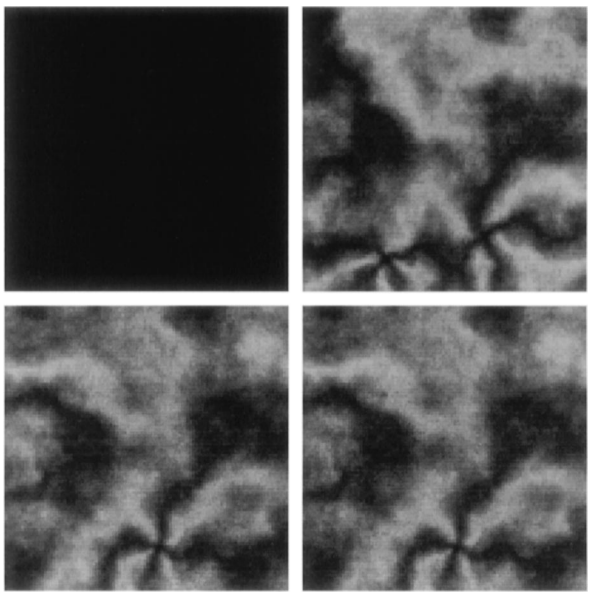

FIG. 1. Cross-polarizer images of the evolution of defects obtained from MC simulations of a $100 \times 100 \times 12$ lattice starting from a perfectly aligned normal configuration after 100 (top left), 6000 (top right), 50 000 (bottom left), 80 000 (bottom right) cycles.

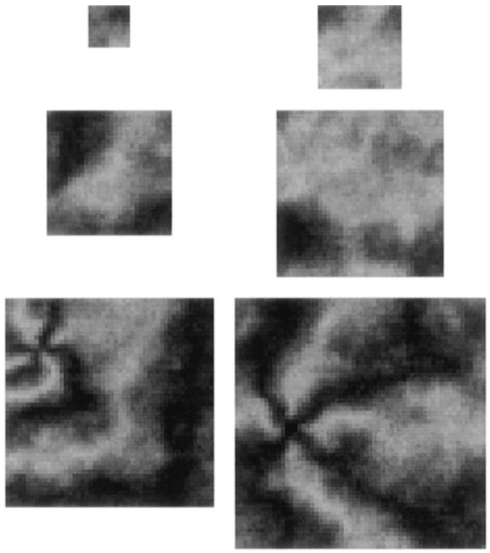

FIG. 2. Cross-polarizer images of the MC configurations for a $10 \times 10 \times 10$, $20 \times 20 \times 10$, $30 \times 30 \times 10$, $40 \times 40 \times 10$, $50 \times 50 \times 10$, and $60 \times 60 \times 10$ after the same number of evolution cycles (10^5) shown from the smallest (top left) to largest (bottom right).

FIG. 3(color). A three dimensional representation of the MC molecular organization of a $10 \times 10 \times 10$ lattice showing the uniform configuration reached for this small sample. The molecular orientations are color coded to show the preferred direction (yellow). Colors are assigned to five equal intervals of $1 \geq |\mathbf{u} \cdot \mathbf{n}| \geq 0$: yellow (director), cyan, green, red, blue.

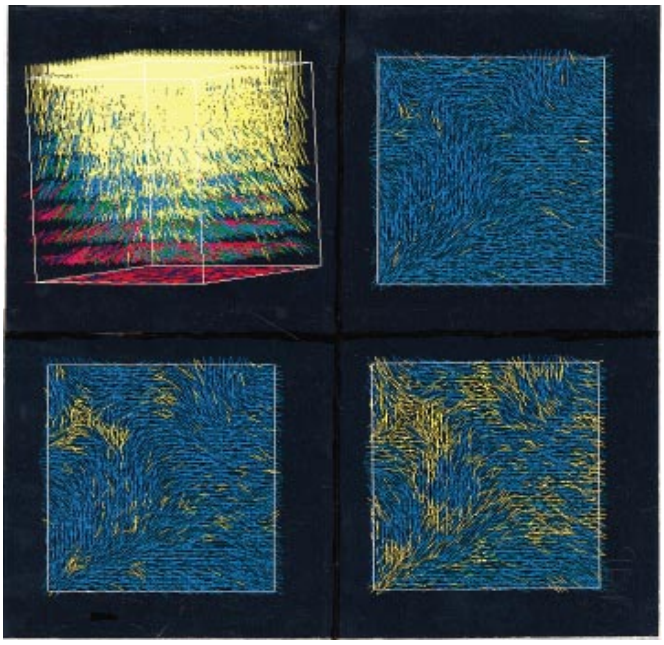

FIG. 4(color). A three dimensional representation of the MC molecular organization showing a $25 \times 25 \times 10$ portion of the $50 \times 50 \times 10$ sample containing the defect (top left). The color coding is the same as in Fig. 3. The other three plates show the first (top right), second (bottom left), and third (bottom right) fluid layers from the bottom surface. Molecules are color coded yellow when almost oriented along z ($|u_z| > 0.7$) and cyan otherwise.

located at the lower surface; the distortions vanish as one moves towards the upper plate and the molecules reorient along the z axis. Note that the results described above are specifically related to the hybrid alignment of the film. In this case the order parameter $\langle P_2 \rangle_\lambda$ (see, e.g., [12]) across the film changes substantially for the larger lattices but not for the small ones (see Fig. 5). Computer simulations with identical boundary conditions at the top and bottom plates reveal no defects: the system relaxes into a uniform nematic and orthogonal planar BC give a uniform twisted structure [19]. Furthermore, when one starts simulations with antagonistic boundary conditions but uniform (in the x, y plane) film, the system develops horizontal deformations, indicating that the uniform HAN state is unstable with respect to the horizontally deformed state.

A striking result of the MC simulations is that the model based exclusively on pure nearest-neighbor molecular interactions mimics the long-range deformations with topologically stable defects. Below we show that the MC results agree with the trends predicted by a macroscopic elastic theory. From the point of view of the macroscopic theory, the LL potential corresponds to one-constant approximation in which splay, twist, and bend elastic constants have the same value K and the divergence elastic constants vanish. Then the elastic-free energy of the nematic liquid crystal is simply

$$\mathcal{F} = \frac{1}{2} K \int dV[(\mathrm{div}\mathbf{n})^2 + (\mathrm{curl}\mathbf{n})^2], \qquad (2)$$

where $\mathbf{n}$ is the nematic director. This one-constant potential suggests that the defect states can be energetically preferable as compared to the defect-free distribution with director uniform in the (x, y) plane. The configurations have different dependence on the characteristic lengths of the system. The uniform HAN structure, $n_x = \sin\theta(z)$, $n_y = 0$, $n_z = -\cos\theta(z)$, $\theta(z) = \theta_1 - \alpha z/h$, $\alpha = (\theta_1 - \theta_2)$, is distorted only in

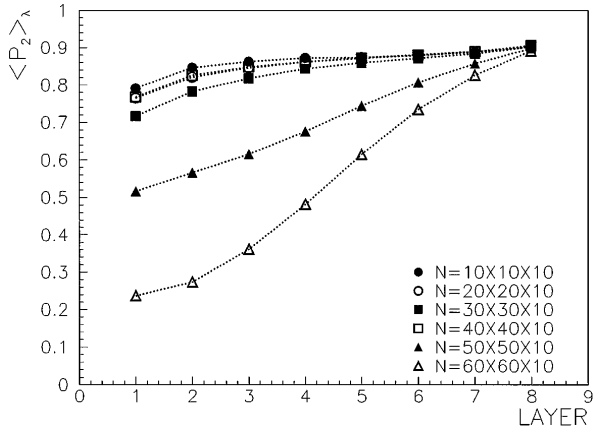

FIG. 5. The MC order parameter $\langle P_2 \rangle_\lambda$ across the sample for the various films studied. The lattice size and the corresponding symbols are as indicated.

the vertical plane, because of the difference in the polar angles $\theta_1 = \pi/2$ and $\theta_2 = 0$ of the director at the bottom and top surfaces, respectively (strong anchoring). As a result, the elastic energy of a round HAN film of radius $R \sim L$ with director uniform in the (x, y) plane scales as R^2/h: $\mathcal{F}_0 = \pi^3 K R^2/8h$. In contrast, the states with topological defects are distorted also in the horizontal plane and their energy contains two additional terms that scale linearly and logarithmically with R. Consider, for example, an $m = 1$ defect in approximation that the vertical and horizontal distortions are decoupled [which can be justified only far away from the defect core, i.e., for large R/h], $n_x = \sin\theta(z)\cos(\phi + c)$; $n_y = \sin\theta(z)\sin(\phi + c)$; $n_z = -\cos\theta(z)$. Here ϕ is the azimuthal angle in the x, y plane, and c is the constant that controls the radial vs cylindrical distribution around the defect. Using Eq. (2) one finds the energy of the defect state as

$$\mathcal{F}_1 = \frac{\pi}{8} K[\pi^2 R^2/h - 4\pi R\cos c + 4h\ln(R/r_c)] + \mathcal{F}_c, \quad (3)$$

where r_c and $\mathcal{F}_c$ are the radius and the energy of the defect core, respectively. Note that r_c and $\mathcal{F}_c$ for the surface $m = 1$ defect are defined by both bulk and surface anchoring parameters and also depend on c. At first sight, the constant c should be put equal to 0, which would correspond to a radial in-plane configuration. However, this trend can be altered by the dependency of $\mathcal{F}_c$ on c. The comparison of the various contributions to $\mathcal{F}_1$ shows that the term linear in R is responsible for the energy save. For sufficiently large R/h, this term can overcome the logarithmic term and make the defect state energetically more preferable than the uniform (in the x, y plane) HAN structure, $\mathcal{F}_1 - \mathcal{F}_0 < 0$.

When the film is confined between two planes with identical BC, $\alpha = 0$, the linear term does not appear and there is no reason for the defect to be stable. In other words, the defects are stabilized by the balance of the surface anchoring and the bulk elasticity. Thus the MC simulation follows the qualitative trends predicted by the elastic theory arguments. Of course, a complete comparison of the continuum and microscopic approach is difficult because of a complex 3D geometry of the structures; see Figs. 1–4.

To conclude, we performed MC simulations of thin nematic films bounded by two plates with antagonistic normal and tangential orientation of molecules. These boundary conditions *per se* do not guarantee the appearance of stable defects: from the point of view of topology, the system is trivial. However, the ground state of the MC simulated system contains stable topological defects. Physically the effect can be understood as a balance of surface anchoring that creates director distortions across the cell and nematic elasticity that responds by deformations in the plane of the cell. We believe that further enlargement of the simulated system would allow a direct comparison with periodic structures of defects observed experimentally [20].

We thank NATO for CRG 961264 that made this work possible and Regione Emilia-Romagna CED for the use of DEC AXP 7000-710. C. Z. thanks MURST, CNR, and University of Bologna for support. O. D. L. acknowledges NSF ALCOM Center Grant No. DMR-20147.

[1] M. Kleman, *Points, Lines and Walls* (Wiley, New York, 1983).
[2] A. J. Bray, Physica (Amsterdam) **194A**, 41 (1993).
[3] W. H. Zurek, Nature (London) **382**, 296 (1996).
[4] S. Renn and T. Lubensky, Phys. Rev. A **38**, 2132 (1988).
[5] R. Kamien and D. Nelson, Phys. Rev. E **53**, 650 (1996).
[6] S. Meiboom, J. Sethna, P. W. Anderson, and W. F. Brinkman, Phys. Rev. Lett. **46**, 1216 (1981).
[7] O. D. Lavrentovich, Sov. Phys. JETP **64**, 984 (1986).
[8] P. Poulin, H. Stark, T. C. Lubensky, and D. A. Weitz, Science **275**, 1770 (1997).
[9] O. D. Lavrentovich and V. M. Pergamenshchik, Int. J. Mod. Phys. B **9**, 2389 (1995).
[10] C. Chiccoli, P. Pasini, F. Semeria, T. J. Sluckin, and C. Zannoni, J. Phys. II (France) **5**, 427 (1995).
[11] P. A. Lebwohl and G. Lasher, Phys. Rev. A **6**, 426 (1972).
[12] U. Fabbri and C. Zannoni, Mol. Phys. **58**, 763 (1986).
[13] E. Berggren, C. Zannoni, C. Chiccoli, P. Pasini, and F. Semeria, Phys. Rev. E **50**, 2929 (1994).
[14] M. P. Allen and D. J. Tildesley, *Computer Simulation of Liquids* (Oxford University Press, Oxford, 1987).
[15] R. Ondris-Crawford, E. P. Boyko, B. G. Wagner, J. H. Erdmann, S. Žumer, and J. W. Doane, J. Appl. Phys. **69**, 6380 (1991).
[16] F. Xu, H.-S. Kitzerow, and P. P. Crooker, Phys. Rev. A **46**, 6535 (1992).
[17] A. Kilian, Liq. Cryst. **14**, 1189 (1993).
[18] C. Chiccoli, P. Pasini, F. Semeria, E. Berggren, and C. Zannoni, Mol. Cryst. Liq. Cryst. **266**, 241 (1995).
[19] C. Chiccoli, P. Pasini, F. Semeria, E. Berggren, and C. Zannoni, Int. J. Mod. Phys. C **6**, 135 (1995).
[20] O. D. Lavrentovich and Yu. A. Nastishin, Europhys. Lett. **12**, 135 (1990).